

Observation of chaotic itinerancy in the light and carrier dynamics of a semiconductor laser with optical feedback

Will Ray,^{1,2} Wing-Shun Lam,^{1,2} Parvez N. Guzdar,² and Rajarshi Roy^{1,2,3}
¹*Department of Physics, University of Maryland, College Park, Maryland, 20742, USA*
²*IREAP, University of Maryland, College Park, Maryland 20742, USA*
³*IPST, University of Maryland, College Park, Maryland 20742, USA*
 (Received 7 June 2005; published 23 February 2006)

We report a direct experimental observation of chaotic itinerancy in simultaneous measurements of the light intensity and voltage fluctuations of a laser diode exhibiting low-frequency fluctuations. The distribution of trajectories leading up to (following) an intensity dropout is computed from the experiment and reveals the presence of itinerant mechanisms before (after) dropout initiation. A phase space reconstruction of the trajectory for the optimal path of motion illustrates sudden shifts between low-dimensional attractor ruins and is shown to correspond to simulations of the laser intensity and carrier number.

DOI: 10.1103/PhysRevE.73.026219

PACS number(s): 05.45.Jn, 42.65.Sf, 42.55.Px

Chaotic itinerancy (CI) has recently been proposed as a ubiquitous phenomenon in a variety of high-dimensional dynamical systems and is generally recognized as itinerant switching between low-dimensional attractors via high-dimensional chaos [1]. Experiments and numerical models of nonlinear coupled oscillators [2] and systems with time-delayed feedback [3], in particular, have contributed largely to the characterization of this dynamic mechanism. Optical media under the influence of delayed feedback have served as exemplary systems for studying manifestations of CI [4], and itinerant motion has been found to be relevant in describing the dynamical behavior of photorefractive cells [5] and laser systems exhibiting multimode oscillations [6].

A semiconductor laser under the influence of reflective optical feedback may display a wide variety of dynamical states over a large range of feedback strengths. Analysis of the delay-differential equations [7] governing this system predict an itinerant motion among external cavity modes and unstable saddles, resulting in sudden dropouts of the laser intensity [8,9]. These dropout events occur irregularly at an average time scale that is much slower than the intrinsic time scales of the light dynamics and are commonly referred to as low-frequency fluctuations (LFF).

Identification of CI is especially difficult in experiments, where typically only one scalar variable may be measured directly. Streak camera measurements of the light dynamics on very short time scales have provided indirect confirmation of the deterministic scenario of LFF predicted from the numerical model [10]. Hilbert phase information extracted from filtered intensity measurements has previously demonstrated external cavity mode shifts [11].

For the present study, we are interested in characterizing the itinerant motions displayed in *simultaneous measurements of the light and carrier dynamics* during the course of a dropout event. In order to elicit features common to many individual dropouts, we form a statistical description of the process from a large number of dropouts by calculating the experimental prehistory and posthistory probability distribution functions [12] for the intensity and voltage fluctuations across the laser diode. Optimal paths extracted from the

probability distributions serve as the building blocks to reconstruct the phase space dynamics of the dropout event. The resulting trajectory highlights episodic transitions between low-dimensional attractor ruins [1] and demonstrates excellent agreement with simulations of the intensity and carrier number.

The dynamics of LFF in the active region of the laser has been extensively studied in the framework of the single-mode Lang-Kobayashi rate equations [7], given below in a slightly different form [11]:

$$\frac{dE}{dt} = \frac{1}{2}(1 + i\beta_c)G_N n E(t) + \kappa E(t - \tau)e^{-i\omega_0\tau} + F_E(t), \quad (1)$$

$$\frac{dn}{dt} = (P - 1)\frac{N_{th}}{\tau_r} - \Gamma|E|^2 - n\left(\frac{1}{\tau_r} + G_N|E|^2\right). \quad (2)$$

Here $E(t) = |E(t)|e^{i\phi(t)}$ is the complex optical field; $n(t) \equiv [N(t) - N_{th}]$ is the difference between the carrier number at arbitrary time and the threshold carrier number N_{th} ; β_c is the linewidth enhancement factor; G_N is the differential gain and τ is the external cavity round trip time; ω_0 is the solitary laser frequency and P is the ratio of pump and threshold currents; $F_E(t)$ is the Langevin noise term, with $\langle F_E(t)F_E(t')^* \rangle = R_{sp}\delta(t-t')$, where R_{sp} is the spontaneous emission rate; τ_r denotes the carrier recombination time and Γ signifies the photon decay rate.

For a given effective feedback rate κ , the steady states of Eqs. (1) and (2) define a set of fixed points in terms of the intensity $|E|^2$, carrier number difference, and external cavity phase shift $\eta(t) \equiv [\phi(t) - \phi(t - \tau)]$. As the feedback strength is increased, new fixed points are created via a saddle-node bifurcation while existing stable attractors destabilize into locally coupled attractor ruins [8]. The resulting dynamics of this system is traditionally viewed in the $(\eta(t), n(t))$ phase space, where the fixed points lie on a tilted ellipse [13]. As the trajectory wanders among the chaotic attractors close to the maximal gain mode at the tip of the ellipse, a crisis occurs when the system gets too close to the saddle nodes

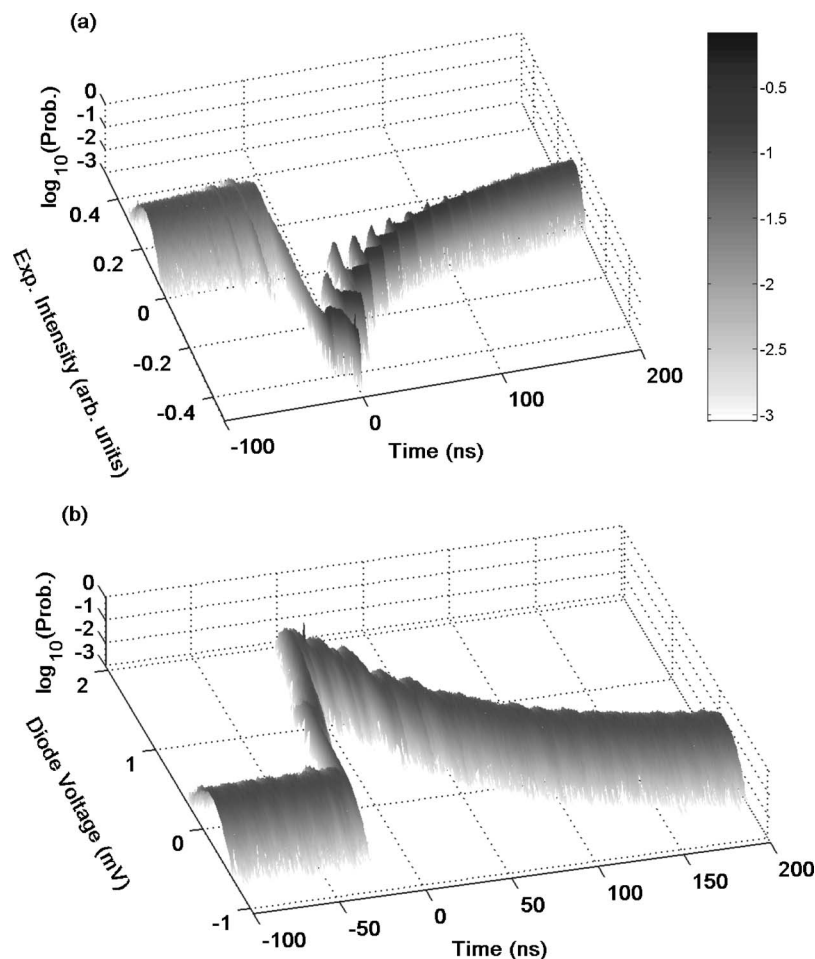


FIG. 1. (a) The logarithm of the prehistory and posthistory probability distribution function (color coded as shown) of experimental intensity dropouts with $t=0$ at the bottom of the dropout. (b) The logarithm of the prehistory and posthistory probability distribution of diode voltage pulses corresponding to the intensity dropouts in (a).

(antimodes) on the upper branch. This initiates a sudden shift in $\eta(t)$ and $n(t)$ to solitary lasing conditions (i.e., without feedback), coincident with the dropout of intensity. A step-wise, itinerant recovery of the system variables towards maximum gain follows along the lower branch of the ellipse [8]. We directly measure the dominant itinerant mechanisms present in the intensity and carrier number during the time evolution of the dropout.

In the experiment, a temperature controller is used to stabilize (to better than 0.01 K) a Fabry-Perot semiconductor laser (RLT8340). The light ($\lambda=830$ nm) from the laser is reflected by a mirror placed at a distance of 214 cm from the antireflection-coated facet. A beam splitter directs light onto a photodetector (12 GHz bandwidth). The output of the photodetector is recorded by a digital oscilloscope with 200 ps resolution and a 1 GHz bandwidth. The laser is pumped with a bias current of 48.7 mA, which is 1.01 times of the threshold current, and is subjected to a feedback that reduces the threshold current by about 10%.

Concurrent measurements of the intensity from the photodetector and the voltage fluctuations across the laser diode indicate that the diode voltage exhibits pulsations when the intensity has power dropouts—they occur *simultaneously*, an observation [14] first made only a few years after the discovery of LFF [15]. These voltage fluctuations represent changes in the current (carrier number) across the laser diode [16]. We note that a 24 ns oscillation inherent to the elec-

tronic loop involved in voltage detection is present independent of the external cavity delay time. The effect of the electronics is deconvoluted by passing the measured voltage through a notch filter RLC circuit [17].

Each dropout pulse evolves in a similar manner, and characteristics of the dropout process may be deduced statistically. Previous studies have examined the recovery process [18] and the role of relaxation oscillations [19]. Here we extract itinerant motions significant to a large number of dropouts by adopting a methodology [12] commonly used to study escape dynamics in the theory of large fluctuations. The distribution of trajectories leading to escape from a metastable state generally displays a distinct peak, known as the optimal path, indicating how the system is most likely to move. In the context of large fluctuations, the motion and variance of this optimal path gives insight to the potential barrier crossed during activated escape [20]. For the purposes of our study, the optimal path reveals epochs before and after the dropout where the system dynamics is dominated by high-dimensional transitions between external cavity modes.

The prehistory ($t<0$) and posthistory ($t>0$) probability distribution functions constructed from 718 intensity dropout events in the experiment are shown in Fig. 1(a), where the moment of dropout ($t=0$) is referenced at the lowest point of a given dropout pulse evolution. The average intensity of the entire time series has been subtracted and the probability of a

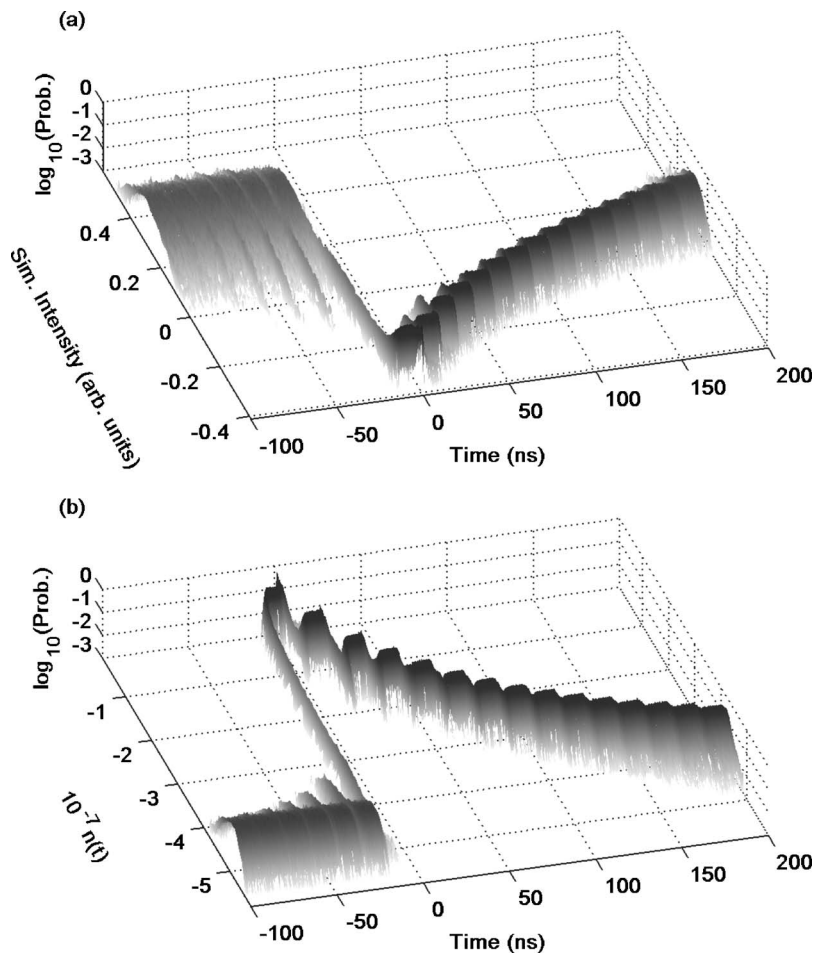


FIG. 2. (a) The logarithm of the prehistory and posthistory probability distribution of simulated intensity dropouts. (b) The logarithm of the prehistory and posthistory probability distribution of carrier number difference corresponding to the intensity dropouts in (a).

particular intensity at a given time instant is presented logarithmically to clearly display the variation of trajectories outside the optimal path.

The prehistory distribution reveals the behavior of the system immediately before the dropout. Far from the dropout, there is no structure in the dynamics, and the optimal path lies along the average maximal output. Right before the intensity drops, however, several periodic build-up spikes are visible with a period which is one external cavity round trip time. In the posthistory distribution, a stair structure is clearly visible with a stair width of one round trip time [18]. As the intensity recovers close to the maximal output region, the stairs become indistinguishable.

Figure 1(b) displays the prehistory and posthistory distribution for the pulses of the deconvoluted diode voltage corresponding to the intensity dropouts in Fig. 1(a). In the prehistory, no build-up structure may be resolved, and we observe a rise in the pulse to full height. The posthistory distribution shows the gradual decay of the voltage fluctuation, modulated at the round trip time period.

The experiment may be numerically modeled by integrating Eqs. (1) and (2) with a time step of 0.5 ps for the following parameter values: $N_{th}=3.3 \times 10^8$, $\beta_c=5$, $G_N=7176 \text{ s}^{-1}$, $\tau=14.2 \text{ ns}$, $R_{sp}=5 \times 10^{13} \text{ s}^{-1}$, $\tau_r=1.1 \text{ ns}$, $\Gamma=1.2 \text{ ps}^{-1}$, $\kappa=2 \times 10^{11} \text{ s}^{-1}$, $P=1.01$. The calculations are low-pass filtered and smoothed over intervals of 0.2 ns to simulate the digital oscilloscope electronics.

In Fig. 2, the prehistory and posthistory distributions for the intensity and the carrier number from the simulation are plotted. In Fig. 2(a), all structures shown in the experimental distribution of Fig. 1(a) are accurately reproduced. The distribution in Fig. 2(b) clearly depicts the characteristic stair structure and periodic build-up spikes. The flat portions of the optimal trajectory for the distributions in Figs. 1 and 2 correspond to the residence of the system in an external cavity mode. However, at intervals of the external cavity round trip time, the optimal path demonstrates large swings which indicate the most likely excursion taken by the system variables in transit to the next low-dimensional lasing mode. In Fig. 3(a), we build the phase space dynamics from the experiment using the optimal intensity and deconvoluted diode voltage from the distributions in Fig. 1. Similar dynamics are constructed in Fig. 3(b) using the optimal intensity and carrier number from Fig. 2. The modes [(blue online) triangles] and antimodes [(red online) circles] in this representation lie interlaced along a curve. Before the dropout, the trajectory resides in the high gain modes at the top of the curve. The trajectory traverses the phase space during the pulse and iteratively recovers along a series of external cavity modes, clearly depicting in-step itinerant transitions of the intensity and carrier dynamics.

During an itinerant epoch, the system variables released from a local attractor are temporarily free to occupy a larger volume of phase space until the system locks onto another

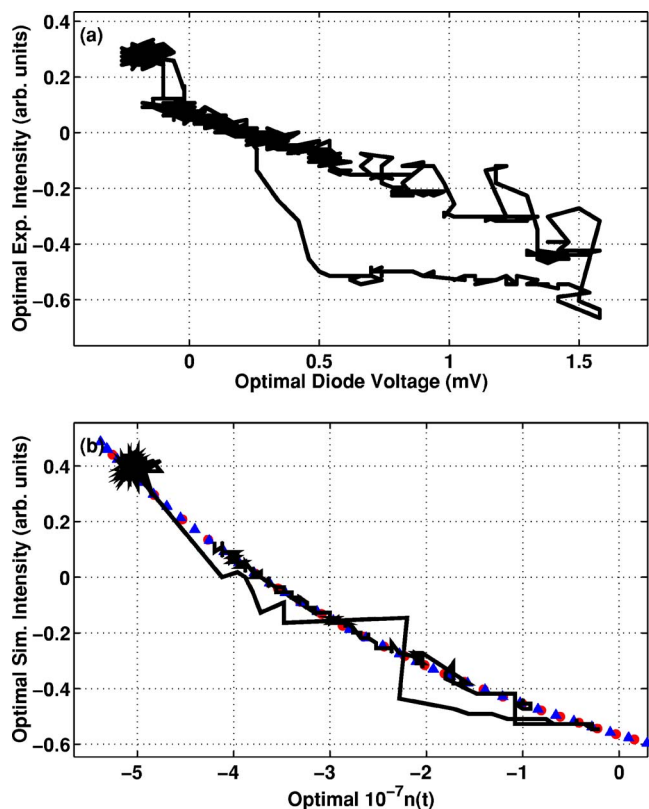


FIG. 3. (Color online) (a) Experimental dynamics in the phase space of optimal measured dropout intensity versus diode voltage. (b) Computational dynamics in the phase space of optimal simulated dropout intensity versus deconvoluted carrier number difference. The (blue online) triangles represent external cavity modes and the (red online) circles denote antimodes of the Lang-Kobayashi equations.

low-dimensional external cavity mode. The increase in available system phase space results in a significant broadening of the probability distributions computed for measurements of the light intensity and carrier number. This variation is illustrated concretely in Fig. 4, where we plot the time dependence of the standard deviation of the measured and calculated distributions in Figs. 1 and 2. Sharp rises in the standard deviation of the distributions occur at intervals of the external cavity round trip time, where high-dimensional dynamics dominate the motion of the feedback system. These distributions show that itinerant motions are present both before and after the dropout events. This observation cannot be explained by a simplified one-dimensional sto-

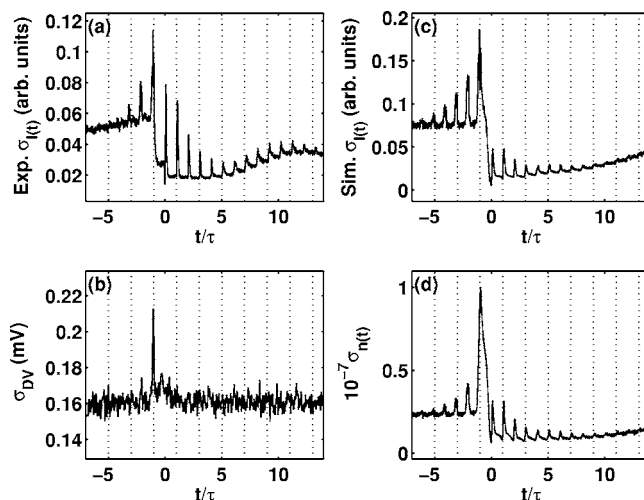


FIG. 4. The standard deviation σ of the probability distributions of (a) experimental intensity dropouts, (b) diode voltage pulses, (c) computational intensity dropouts, and (d) carrier number difference. Time is displayed in units of the external cavity delay time τ .

chastic model [13,20] of fluctuation-induced escape. The deterministic structure observed before the dropout implies that the itinerant deviations are reinforced over many round trip times until the dropout finally occurs.

In conclusion, we have reported experimental observations of concurrent itinerant motions in the light and carrier dynamics of a semiconductor laser under the influence of reflective feedback. These measurements are consistent with the predictions of the Lang-Kobayashi equations. The role of CI in the time evolution surrounding an intensity dropout is evaluated in detail using prehistory and posthistory probability distributions calculated from experimental measurements of the intensity and voltage fluctuations across the diode. At intervals of the external cavity round trip time, the system variables are no longer locally constrained to a low-dimensional external cavity mode. Despite this loss of coherence in the light and carrier dynamics, a continuous optimal path of escape to another attractor ruin is evidenced in the reconstructed phase portrait of the dropout process. This path demonstrates a certain determinism of motion through high-dimensional phase space in the dynamics of a time-delayed experimental system that is additionally influenced by noise.

We gratefully acknowledge support from the Office of Naval Research (Physics) and thank M. I. Dykman and J. Rodgers for helpful discussions.

- [1] K. Kaneko and I. Tsuda, eds., *Chaotic Itinerancy*, focus issue, *Chaos* **13**, 926 (2003).
- [2] K. Kaneko, *Physica D* **41**, 137 (1990); I. Tsuda, *World Futures* **32**, 167 (1991).
- [3] K. Ikeda, K. Otsuka, and K. Matsumoto, *Prog. Theor. Phys. Suppl.* **99**, 295 (1989).
- [4] Zhao Hong, Liu Yaowen, Wang Yinghai, and Hu Bambi, *Phys.*

Rev. E **58**, 4383 (1998).

- [5] F. T. Arecchi, G. Giacomelli, P. L. Ramazza, and S. Residori, *Phys. Rev. Lett.* **65**, 2531 (1990).
- [6] K. Otsuka, T. Ohtomo, T. Maniwa, H. Kawasaki, and Ko, *Chaos* **13**, 1014 (2003).
- [7] R. Lang and K. Kobayashi, *IEEE J. Quantum Electron.* **QE-16**, 347 (1980).

- [8] T. Sano, Phys. Rev. A **50**, 2719 (1994).
- [9] G. H. M. van Tartwijk, A. M. Levine, and D. Lenstra, IEEE J. Sel. Top. Quantum Electron. **1**, 466 (1995).
- [10] I. Fischer, G. H. M. van Tartwijk, A. M. Levine, W. Elsasser, E. Gobel, and D. Lenstra, Phys. Rev. Lett. **76**, 220 (1996).
- [11] W. S. Lam, P. N. Guzdar, and R. Roy, Phys. Rev. E **67**, 025604(R) (2003).
- [12] M. I. Dykman, P. V. E. McClintock, V. N. Smelyanski, N. Stein, and N. G. Stocks, Phys. Rev. Lett. **68**, 2718 (1992).
- [13] C. H. Henry and R. Kazarinov, IEEE J. Quantum Electron. **QE-22**, 294 (1986).
- [14] R. Ries and F. Sporleder, in *Proceedings of the 8th European Conference on Optical Communication, Cannes, France, 1982* (Comité de la Conférence Européenne sur les Communications Optiques, Cannes, 1982), p. 285; as referenced in K. Petermann, *Laser Diode Modulation and Noise* (Kluwer, Dordrecht, 1988), p. 281.
- [15] C. Risch and C. Voumard, J. Appl. Phys. **48**, 2083 (1977).
- [16] The time scales of the LFF are too fast to be controlled by the laser power supply, and so the diode voltage fluctuations are a good representation of the population inversion dynamics.
- [17] The electronics loop consists of a parallel measurement of the laser diode and laser power supply through a BNC connector. In the model RLC circuit C is in parallel to the serial connection of L and R, and the values of L and C are optimally chosen with a resonant frequency of the uncharacteristic 24 ns. A 281 MHz low-pass filter removes high frequencies incurred in the transformation.
- [18] Y. Liu, P. Davis, and Y. Takiguchi, Phys. Rev. E **60**, 6595 (1999).
- [19] G. Huyet S. Hegarty, M. Gludici, B. de Bruyn, and J. G. McInerney, Europhys. Lett. **40**, 619 (1997); S. P. Hegarty, G. Huyet, P. Porta, and J. G. McInerney, Opt. Lett. **23**, 1206 (1998).
- [20] J. Hales, A. Zhukov, R. Roy, and M. I. Dykman, Phys. Rev. Lett. **85**, 78 (2000).